Optimization of Permalloy Properties for Magnetic Field Sensors Using He^+ Irradiation

G. Masciocchi,[1,2,*] J.W. van der Jagt,[3,4] M.-A. Syskaki,[1,5] J. Langer,[5] G. Jakob,[1] J. McCord,[6,7] B. Borie,[3] A. Kehlberger,[2] D. Ravelosona,[3,8] and M. Kläui[1,†]

[1] *Institute of Physics, Johannes Gutenberg University Mainz, Staudingerweg 7, 55128 Mainz, Germany*
[2] *Sensitec GmbH, Walter-Hallstein-Straße 24, 55130 Mainz, Germany*
[3] *Spin-Ion Technologies, 10 boulevard Thomas Gobert, 91120 Palaiseau, France*
[4] *Université Paris-Saclay, 3 rue Juliot Curie, 91190 Gif-sur-Yvette, France*
[5] *Singulus Technologies AG, Hanauer Landstraße 107, 63796 Kahl am Main, Germany*
[6] *Faculty of Engineering, Institute for Material Science, Synthesis and Real Structure, Kiel University, Kaiserstraße 2, 24143 Kiel, Germany*
[7] *Kiel Nano, Surface and Interface Science (KiNSIS), Kiel University, Christian-Albrechts-Platz 4, 24118 Kiel, Germany*
[8] *C2N, CNRS, Université Paris-Saclay, 10 boulevard Thomas Gobert, 91120 Palaiseau, France*

(Received 1 March 2023; revised 5 May 2023; accepted 8 June 2023; published 5 July 2023)

Permalloy, despite being a widely used soft magnetic material, still requires optimization in terms of magnetic softness and magnetostriction for its use in magnetoresistive-sensor applications. Conventional annealing methods are often insufficient to locally achieve the desired properties for a narrow parameter range. In this study, we report a significant improvement in the magnetic softness and magnetostriction in a 30-nm permalloy film after He^+ irradiation. The irradiation treatment reduces the induced anisotropy by a factor of 10 and the hard-axis coercivity by a factor of 5 compared with the values in the as-deposited state. In addition, the effective magnetostriction of the film is significantly reduced by a factor ten (below 1×10^{-7}) after irradiation. All the above-mentioned effects can be attributed to the isotropic crystallite growth of the $Ni_{81}Fe_{19}$ alloy and to the intermixing at the magnetic layer interfaces under light-ion irradiation. We support our findings with X-ray-diffraction analysis of the textured $Ni_{81}Fe_{19}$ alloy. Importantly, the sizable magnetoresistance is preserved after the irradiation. Our results show that compared with traditional annealing methods, the use of He^+ irradiation leads to significant improvements in the magnetic softness and reduces strain cross-sensitivity in permalloy films required for 3D positioning and compass applications. These improvements, in combination with the local nature of the irradiation process, make our findings valuable for the optimization of monolithic integrated sensors, where classic annealing methods cannot be applied due to complex interplay within the components in the device.

DOI: 10.1103/PhysRevApplied.20.014001

I. INTRODUCTION

Permalloy, a typical soft magnetic $Ni_{81}Fe_{19}$ alloy, is used as an active sensor layer in several magnetoresistive-sensor applications [1]. To have a small magnetostriction and low coercivity, most of these devices are designed around the alloy composition of $Ni_{81}Fe_{19}$, which also possesses significant anisotropic magnetoresistance (AMR). Optimization of permalloy for AMR sensors has been studied for a long time [2–4] and includes different aspects: primarily, improvement of magnetic softness and low magnetostriction. To achieve that, negligible crystalline anisotropy is firstly required. The single thin-film elements typically feature a stripe-shaped geometry to induce a strong shape anisotropy, providing the sensor with a well-defined orientation of sensitivity. Furthermore, this design of the sensitive elements ensures a fixed configuration of the magnetic domains, thus enabling a very high signal-to-noise ratio. Additional anisotropies of other sources, if not oriented in the same direction as the shape anisotropy, would hinder this directional sensitivity [5]. Moreover, to achieve low hysteresis, the coercivity in the hard-axis magnetization direction must be very low and the specific AMR must be as high as possible [6] to maximize sensitivity. Finally, to avoid parasitic anisotropies, low magnetostriction (source of magnetoelastic anisotropy) is required. In this case, strain in the

*gmascioc@uni-mainz.de
†klaeui@uni-mainz.de

material has a small or negligible impact on the magnetic properties. The low magnetoelastic anisotropy is particularly important for sensors on flexible substrates [1,7–10], which have attracted great interest in recent years in wearable electronics and biomedical applications. To obtain this particular material property, growth optimization [11] and annealing [12] are viable options. However, none of these techniques allows a local treatment of the film properties.

Ion irradiation is an excellent tool to tune locally the magnetic and structural properties of thin films through ordering [13–16] and interface intermixing [17–20]. In permalloy films, ion irradiation has been shown to change the magnetic anisotropy [21–23] and the magnetoresistive response in the presence of exchange bias [4,24]. However, most of these studies used ion implantation [25–27], high ion energies [28,29], or heavy ions [30], which can result in significant damage to the sample. This can be avoided by use of lighter ions—such as He^+—with energies in the range of 10–30 keV [17,31]. In this way, collision cascades are absent and the structural modifications are confined to the vicinity of the ion path in a metal. Furthermore, the effect of irradiation on the magnetoelastic properties of single permalloy films and a direct comparison between field-free ion irradiation and annealing have not yet been reported [32].

In this work, we propose and explore the use of He^+ irradiation on a sputtered layer of $Ni_{81}Fe_{19}$ (30 nm) as material preparation technique for magnetic field sensors and we compare it with standard field-free annealing. Using Kerr microscopy and vibrating-sample magnetometry, we show that 20-keV He^+ ions significantly reduce the coercivity and the induced magnetic anisotropy of our magnetic material. The result is a soft magnetic film with in-plane magnetic anisotropy of less than 10 J/m^3 and a coercive field of approximately 0.05 mT, which is a further improvement over the values that can be obtained by the field-free annealing process by a factor of 5 and 10, respectively. The anisotropy measurements are supported by a detailed comparison using the remanent domain pattern. Additionally, we show that the polycrystalline magnetostriction can be progressively reduced by a factor of 10 for irradiation doses of 5×10^{16} cm^{-2}. This reduction in magnetoelastic coupling is attributed to crystallization and changes to the interface magnetostriction caused by intermixing at the magnetic layer boundaries. We support our findings with structural characterization performed using X-ray diffraction (XRD). The results show an overall improvement in the crystallization after irradiation and annealing. We attribute the reduction in magnetic anisotropy to the absence of a preferential direction of atomic ordering and to stress relaxation during irradiation. As postgrowth He^+ irradiation improves magnetic softness and minimizes strain cross-sensitivity of permalloy, AMR magnetic sensors with high sensitivity and low hysteresis can be envisioned even for integrated devices.

II. EXPERIMENTAL METHODS

The samples are prepared by dc magnetron sputtering using a Singulus Rotaris system on 1.5-μm-thick, thermally oxidized SiO_x on top of a 625-μm-thick Si substrate. A layer of $Ni_{81}Fe_{19}$ (30 nm)—typical thickness used for various sensor applications—is sputtered at room temperature in the presence of a rotating magnetic field of 5 mT on a Ni-Fe-Cr (5 nm) seed layer and capped with 4 nm of Ta as shown in Fig. 1(b). The following sputtering conditions are used for the magnetic layer growth: base pressure 5×10^{-8} mbar, sputtering power 1200 W, and Ar^+ flow 90 sccm. The seed layer is used to promote a $Ni_{81}Fe_{19}(111)$ texture during growth and it is known to improve magnetoresistance [25,33]. After deposition, optical lithography and ion etching are used to pattern arrays of disks (diameter of 80 μm and spacing of 3 μm) on the samples to probe the local film properties. Multiple copies of the samples are irradiated at an energy of 20 keV with different fluences of He^+ ions from 5×10^{13} to 5×10^{16} cm^{-2}. Under these irradiation conditions, most of the ions reach the substrate (roughly 94% from Monte Carlo TRIM [34,35] simulations), resulting in homogeneous irradiation of the entire layer stack. To process thicker permalloy layers (100 nm), a higher acceleration energy of the ions would be required to obtain comparable irradiation profiles. The results of the TRIM simulations for this case can be found in Sec. S2 in Supplemental Material [36].

To compare the effect of ion irradiation with that of thermal annealing, the same magnetic material is consecutively annealed for 3 h at 200, 265, and 300 °C at a pressure of 10^{-7} mbar. To avoid a magnetization-induced preferential direction of ordering [26,37], external magnetic fields are minimized during the irradiation and annealing steps. The magnetic properties of the thin films are measured by Kerr microscopy and vibrating-sample magnetometry. The magnetic properties of the films are summarized in Table I. Because of the negligible implantation [31], the value of Young's modulus is assumed to be unaffected by our irradiation and annealing step. Electrical measurement of AMR is performed with four contacts in line in the presence of a rotating magnetic field of 10 mT.

To apply strain to our devices, the substrate is bent mechanically with a three-point bending method. As reported in our previous work [39], a tensile and uniaxial strain is generated [40]. Moreover, the strain is uniform in the central area of the sample and thus in the measured region. As the thin films are in total 40 nm thick, we assume that the strain is entirely transferred from the substrate and that shear strain is negligible. Structural modifications caused by ion irradiation and annealing are probed by XRD with use of a Bruker D8 Discover system.

TABLE I. Parameter values of the magnetic materials (thickness 30 nm) after deposition, annealing, and He^+ irradiation. The values without reference are quantified experimentally. Here M_s is the saturation magnetization, K_u is the uniaxial anisotropy constant, H_c is the coercive field, λ_s is the saturation magnetostriction, and Y is Young's modulus. The same value for Y is considered in all cases.

$Ni_{81}Fe_{19}$	M_s (T)	K_u (J/m^3)	H_c (mT)	$\lambda_s \times 10^{-6}$	Y (GPa)
As deposited	0.95(1)	78(5)	0.20(5)	−0.7(1)	200 [38]
Annealing at 265 °C	0.95(1)	70(5)	0.15(5)	+0.04(9)	200 [38]
He^+ 5×10^{16} cm^{-2}	0.91(1)	8(7)	0.05(5)	+0.01(9)	200 [38]

Angular $2\Theta/\Theta$ scans and rocking-curve measurements are performed on 1×1 cm^2 samples.

III. RESULTS AND DISCUSSION

To compare the structural modifications induced by different material treatments on a $Ni_{81}Fe_{19}$ alloy, XRD measurements on the $Ni_{81}Fe_{19}$ (30 nm) film as deposited and after irradiation and annealing are performed and are reported in Fig. 1. Figure 1(a) shows $2\Theta/\Theta$ angular scans of the permalloy film. A well-defined crystalline texture of $Ni_{81}Fe_{19}(111)$ (and its second-order peak) is present for the material in the as-deposited state and persists after irradiation and annealing in all the fluence and temperature ranges explored. The full width at half maximum (FWHM) of the (111) peak can be estimated, and the quantitative values are reported in Sec. S1 in Supplemental Material [36] as a function of the irradiation fluence and the temperature during annealing. In both cases, the FWHM of the (111) peak decreases by about 15% with increasing ion fluence and annealing temperature with respect to the as-deposited case. The crystallite size (or the size of a coherently diffracting domain in the material along the sample thickness) is a fundamental property that can be extracted from the XRD profile [41]. According to the Scherrer equation [42],

$$D = \frac{K\lambda}{\beta \cos\theta}, \tag{1}$$

the size of crystallites is inversely proportional to the FWHM of a diffraction peak. Here $K = 0.9$ is a dimensionless shape factor, D is the crystallite size, $\lambda = 1.5406$ Å is the wavelength of the Cu $K\alpha$ radiation, θ is the diffraction angle, and β is the line broadening at the FWHM of the XRD peak in radians, after subtraction of the instrumental line broadening. As reported in Fig. 1(c), both annealing at $T > 265$ °C and ion irradiation with a fluence greater than 1×10^{16} cm^{-2} increase the size of crystallites in our films. The size of the diffracting domains estimated with use of Eq. (1) is 22(1) nm for the as-deposited case and more than 24(1) nm after the two material treatments. Additionally,

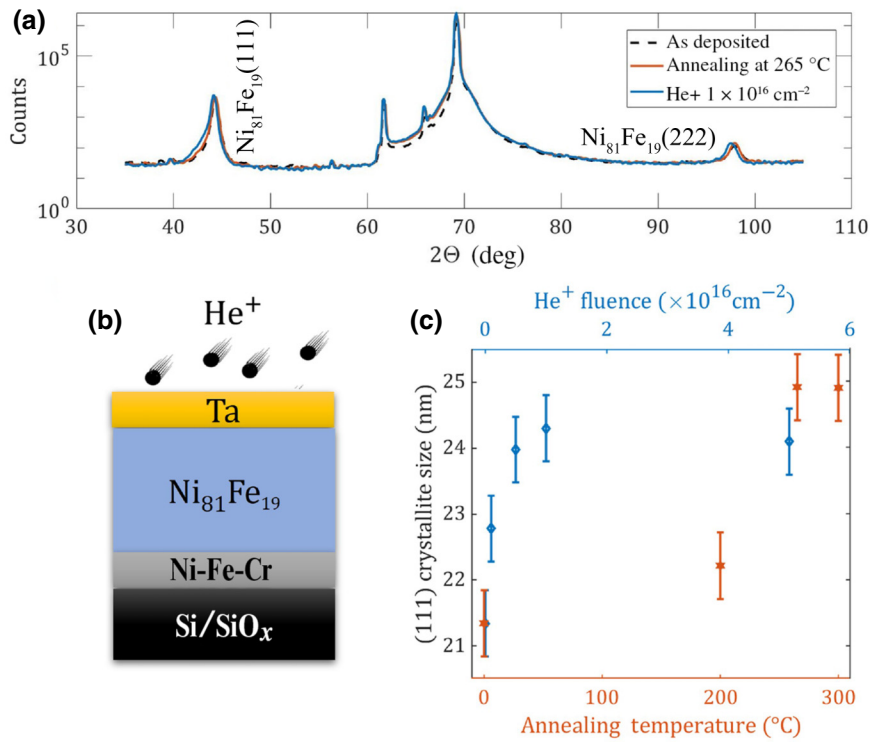

FIG. 1. (a) $2\Theta/\Theta$ XRD angular scan of the $Ni_{81}Fe_{19}$ samples for the sample in the as-deposited state, after annealing and after irradiation. (b) The Ni-Fe-Cr(5 nm)/$Ni_{81}Fe_{19}$(30 nm)/Ta(4 nm) stack. (c) Size of the (111) crystallites of the $Ni_{81}Fe_{19}$ film as a function of He^+ fluence and as a function of annealing temperature. These values are obtained with use of the FWHM of the $Ni_{81}Fe_{19}(111)$ peak and Eq. (1).

rocking-curve measurements [43] of the $Ni_{81}Fe_{19}(111)$ peak are performed, and more information can be found in Sec. S1 in Supplemental Material [36]. For both the irradiated samples and the annealed samples, a decrease in the FWHM of the rocking curve is observed, indicating improvement in the film crystalline phase [44]. As Fig. 1(c) shows, the size of the crystallites does not increase further for annealing temperatures above 265 °C and irradiation fluences greater than 1×10^{16} cm^{-2}, in agreement with previous studies [45].

The major effect of room-temperature irradiation has been shown to be improved material uniformity [46] and interface intermixing [17]. In the same way, thermal annealing is widely used to induce crystallization [47] and promote atomic diffusion [48]. Similar effects have been reported in the literature for amorphous alloys, where annealing [45] and He^+ irradiation [15,16] providing high short-range atomic mobility enable a mechanism for growth of the ordered phase at the expense of its disordered or less-ordered counterpart.

The magnetic properties of the thin films are measured by Kerr microscopy and are reported in Fig. 2. Figures 2(a)–2(c) show the hysteresis curves for the Ni-Fe-Cr(5 nm)/$Ni_{81}Fe_{19}$(30 nm)/Ta(4 nm) sample for two perpendicular in-plane directions of the applied magnetic field: for the as-deposited state [Fig. 2(a)], after annealing [Fig. 2(b)], and after irradiation [Fig. 2(c)]. The curves refer to the magnetic contrast of the structured film into 80-μm-diameter disks.

The magnetic response of the permalloy film in the as-deposited state can be seen in Fig. 2(a). As the magnetization curves at $\Phi = 0°$ and $\Phi = 90°$ are different, a weak uniaxial magnetic anisotropy K_u is present in the as-deposited $Ni_{81}Fe_{19}$ and might be associated with internal stresses during the material growth or asymmetries in the deposition system [49]. $K_u = 80(7)$ J/m^3 is obtained from the area enclosed by easy-axis and hard-axis loops of the as-deposited state. The direction of the magnetic-easy-axis anisotropy can be seen in the orientation of the magnetic domains for the remanent state [inset in Fig. 2(a)]. The field is applied along $\Phi = 0°$ and then reduced to zero. A vector image of the in-plane magnetization is obtained by the sum of the horizontal and vertical components of the magnetic contrast. In this case, the domains align along the easy-axis direction. The measurement is repeated for the same film after annealing and is reported in Fig. 2(b). After the annealing, the in-plane hysteresis loops still show the presence of a uniaxial magnetic anisotropy. This is confirmed by the remanent magnetic state [inset in Fig. 2(b)] as the magnetic domains again orient themselves in the easy-axis direction $\Phi \simeq 90°$. Additional measurements for films annealed at 200 and 300 °C are reported in Sec. S4 in Supplemental Material [36]. Interestingly, the magnetic response of the irradiated permalloy reported in Fig. 2(c) is significantly different with respect to the as-deposited and annealed cases. The change of slope for low fields in the hysteresis in Fig. 2(c) is caused by the formation of a magnetic vortex [shown in the inset in Fig. 2(c)], accompanied by an abrupt decrease in magnetization when the field is decreased from saturation [50]. Additionally, the hysteresis loops now show a negligible angular dependence on Φ. Both the magnetic anisotropy and the hard-axis coercivity H_c are now significantly reduced. The reduction of the anisotropy in the permalloy after irradiation allows the formation of a vortex-type magnetization distribution at remanence, which is energetically favorable for disks with weak crystalline and induced anisotropy [inset in Fig. 2(c)] and thus dominated by shape anisotropy. The hard-axis coercivity H_c is also reduced by irradiation, as the linear motion of the vortex core for low fields in vortex structures minimizes the hysteresis [51].

Figure 2(d) shows the angular plot of the normalized remanent magnetization for the three samples considered. The as-deposited case and the annealed case (in blue and green, respectively) show a signature of uniaxial magnetic anisotropy with easy-axis and sizable remanent magnetization at $\Phi \simeq 90°$. The irradiated sample, instead, shows reduced remanent magnetization for all angles. The low remanent magnetization is typical of the vortex state in the inset in Fig. 2(c). To further understand the improvement in the magnetic softness of our permalloy after irradiation, we gradually increase the He^+ fluence while keeping the ion energy constant. The measurements of H_c and K_u as a function of the fluence of He^+ ions during irradiation are reported in Fig. 2(e). The values for the film as deposited and after annealing are given for comparison as dashed lines. For low fluences, no sizable effects are noted. At fluences greater than 5×10^{13} cm^{-2}, the coercivity and the anisotropy are progressively reduced as the He^+ fluence is increased. For the maximum fluence of 5×10^{16} cm^{-2}, H_c is 5 times lower than for the as-deposited state, while the induced anisotropy is decreased by a factor of 10. We do not observe a similar substantial reduction of these magnetic parameters after the annealing.

A possible explanation for this dissimilarity is the different mechanism of ordering promoted by irradiation and field-free annealing. Improved atomic ordering in permalloy after annealing and irradiation with different ions [30,52] has been reported in the literature. Some of these studies on polycrystalline films [53,54] show that crystalline grain growth is more homogeneous for irradiation than for thermal annealing in the temperature range from 200 to 300 °C. This difference originates from the distinct mechanism with which chemical ordering of the alloy is changed during the two processes [55]. As we see from these studies, radiation-enhanced mobility is more isotropic in the absence of an applied magnetic field when compared with heat-induced mobility [22,55]. Accordingly, a greater reduction in the magnetic anisotropy for the irradiated samples can be expected.

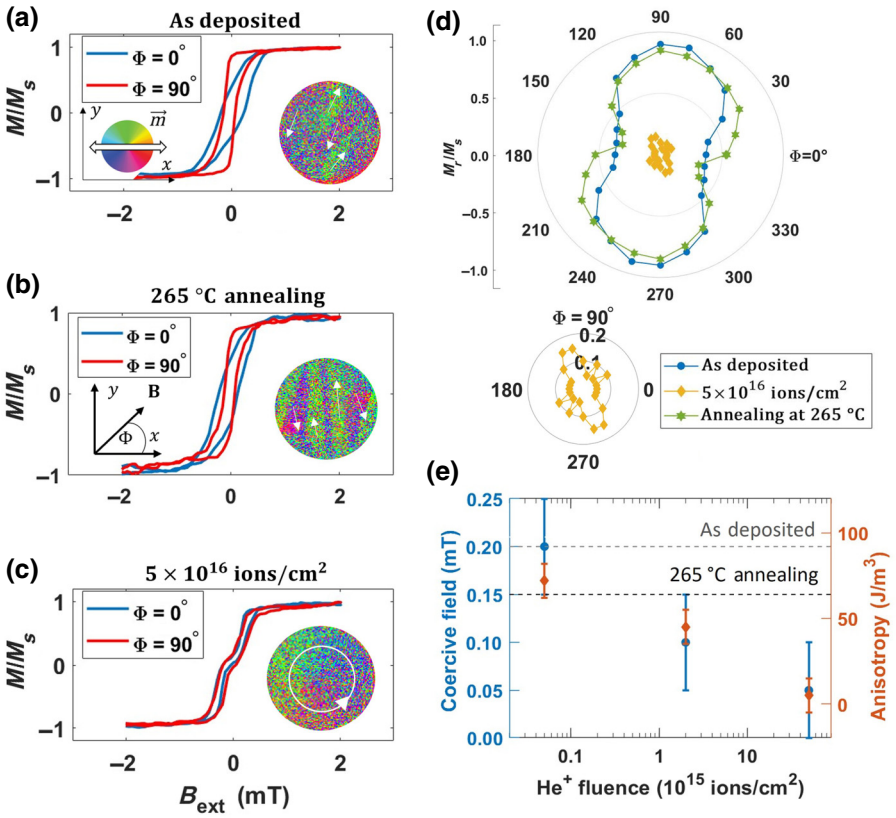

FIG. 2. (a)–(c) In-plane hysteresis loops of Ni-Fe-Cr(5 nm)/$Ni_{81}Fe_{19}$(30 nm)/Ta(4 nm) after sputtering, after thermal annealing, and after He^+ irradiation, respectively. In the insets, the corresponding remanent magnetic state ($B_{ext} = 0$ mT) for 80-μm-diameter disks is shown. The color code corresponds to the in-plane magnetization orientation as indicated by the white arrows. The field is applied along $\Phi = 0°$. (d) Angular plot of the normalized remanent magnetization M_r/M_s as a function of the in-plane magnetic field direction Φ for as-deposited, irradiated, and annealed samples. The measurements after irradiation are highlighted in the inset for clarity. (e) Coercive field (blue) and uniaxial magnetic anisotropy (orange) measured along the field direction $\Phi = 0°$ on a permalloy sample irradiated with different fluences of He^+ ions. For comparison, the values after annealing and in the as-deposited state are reported with dashed lines.

A first indication for the observed reduction in coercivity in our irradiated samples is the formation of a magnetic vortex in disk-patterned permalloy [50] [inset in Fig. 2(c)]. A comparison between ion irradiation and thermal annealing analyzing the microscopic pinning parameters for domain-wall motion was conducted recently [46]. In this work, the annealed sample shows strong but widely distributed pinning sites. In contrast to this, the irradiated sample exhibits weaker defects with a higher density. A further possible explanation for the observed reduction in coercivity in our irradiated samples, is therefore an overall smoother domain-wall energy landscape after irradiation, which allows domain formation and switching of the magnetization at lower magnetic fields. In addition, the release of internal stresses in the film, which has been reported during irradiation [56,57], can also be responsible for improvements in the soft magnetic properties of our permalloy [49].

To evaluate the effect of ion irradiation and annealing on the magnetoelastic coupling of a thin magnetic $Ni_{81}Fe_{19}$ alloy, the strain-dependent magnetic properties are investigated. Uniaxial in-plane strain is applied to a full film of Ni-Fe-Cr(5 nm)/$Ni_{81}Fe_{19}$(30 nm)/Ta(4 nm) by the three-point bending method as previously reported [39]. Since the magnetization is coupled to the external strain via the expression of the anisotropy energy, the magnetic anisotropy before and after the application of strain is measured by Kerr microscopy. A strain of $\epsilon_{xx} = 0.06\%$ (tensile) is applied along the in-plane direction $\Phi = 0°$. The expression for the magnetoelastic anisotropy depends on the saturation magnetostriction λ_s of the material according to [58]

$$K_{ME} = \frac{3}{2}\lambda_s Y \epsilon, \tag{2}$$

where Y is Young's modulus and ϵ is the uniaxial tensile strain. Using Eq. (2) and the values of Young's modulus in Table I, we calculate the effective magnetostriction of the film for different He^+ fluences. The calculated values are reported in Fig. 3(a). In the as-deposited state, as well as for He^+ fluences on the order of 10^{13} cm^{-2}, $\lambda_s = -7(2) \times 10^{-7}$ is negative. In this case, a tensile strain increases the anisotropy field in the direction $\Phi = 0°$. For greater fluences of ions during irradiation, the magnetostriction is progressively reduced and reaches values close to zero for a fluence of 5×10^{16} cm^{-2}. In this case, the magnetoelastic anisotropy is negligible and the material is insensitive to the applied strain. For this reason, the magnetization curves before and after the application of uniaxial strain $\epsilon_{xx} = 0.06\%$ are almost unchanged. The saturation magnetostriction of the magnetic layer after annealing is measured and is reported in Fig. 3(a) for comparison. After the annealing, $\lambda_s \simeq 0$ is reported.

An additional confirmation of the magnetic behavior of the stack under strain is obtained by our imaging domain

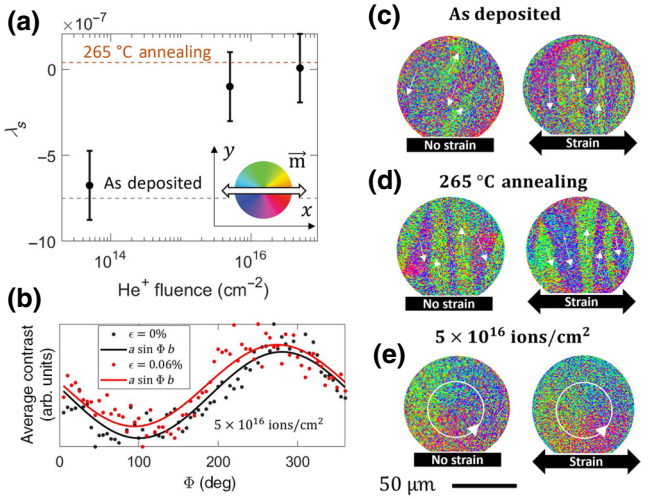

FIG. 3. (a) Saturation magnetostriction λ_s as a function of He^+ fluence during irradiation. The values for the as-deposited sample and the sample after annealing are reported for comparison with dashed lines. (b) Average contrast for 80-μm-diameter disks as a function of the in-plane angle Φ for the irradiated sample in the remanent state (magnetic vortex state) before and after the application of strain. (c)–(e) Remanent magnetic state for 80-μm-diameter disks before (left) and during (right) application of uniaxial strain of 0.06% for as-deposited, annealed, and irradiated permalloy, respectively.

formation using the magneto-optical Kerr effect (MOKE). The MOKE images shown in Figs. 3(c)–3(e) show how the magnetoelastic anisotropy alters the preferential direction of magnetic domains before (left) and after (right) the application of strain. We first consider the as-deposited state [Fig. 3(c)]. Before the application of strain, the magnetization aligns with the deposition-induced anisotropy easy axis. After the application of strain, the negative magnetostriction of the as-deposited sample orients the magnetic domains along the y direction, perpendicular to the uniaxial strain ϵ_{xx}. Figure 3(d) shows, instead, the domain pattern for a sample annealed at 265 °C. In this case the remanent magnetic state is almost not altered by the applied strain. This is in agreement with the extremely low magnetostriction measured, which results in negligible magnetoelastic anistropy $K_{ME} << K_u$. The remanent state for the sample irradiated with a He^+ fluence of 5×10^{16} cm^{-2} [Fig. 3(e)] exhibits instead a magnetic vortex state that is not altered after the application of $\epsilon_{xx} = 0.06\%$. The initial vortex state, unchanged under the application of strain, highlights that the contributions of induced and magnetoelastic anisotropy have been reduced to a point where only the shape anisotropy determines the remanent domain pattern.

To compare more quantitatively the MOKE images and the vortex state of the irradiated sample, the average radial magnetization is calculated from the longitudinal component of the vector image for different in-plane Φ directions [59]. The average contrast is calculated for a single 80-μm-diameter disk for the images in Fig. 3(e) and is reported in Fig. 3(b). For the unstrained state seen on the left in Fig. 3(e), the disk's magnetization is a circularly symmetric vortex, and the average contrast varies periodically with the angular position on the disk. The values well follow the expression $a \sin \Phi b$ [black line in Fig. 3(b)]. After the application of strain, as a consequence of the extremely small magnetostriction, the average contrast [red line in Fig. 3(b)] still follows the periodic behavior $a \sin \Phi b$.

A possible explanation for the reported reduction in saturation magnetostriction after ion irradiation and annealing is the increase in size–probed along the vertical direction—of the crystallites in the Ni-Fe-Cr(5 nm)/$Ni_{81}Fe_{19}$(30 nm)/Ta(4 nm) sample, already highlighted in Fig. 1(c). The magnetostriction of isotropic oriented cubic crystallites can be written as the combination of the saturation-magnetostriction constants λ_{100} and λ_{111} in the (100) and (111) directions, respectively [60]:

$$\lambda_s = \frac{2\lambda_{100} + 3\lambda_{111}}{5}. \tag{3}$$

In permalloy, the two components of the magnetostriction change significantly over the relative Ni and Fe composition range, altering the effective magnetostriction, λ_s. The composition used in this work, $Ni_{81}Fe_{19}$, is predicted to have λ_s close to zero [61]. In our XRD measurement, a 15% reduction of the FWHM of the (111) peak is observed after irradiation and annealing. This crystallization measured along the film thickness can alter the relative contribution of λ_{100} and λ_{111} in the magnetic layer. Following Eq. (3), the effective magnetostriction of the film is changed. As shown in Fig. 3(a), the magnetostriction is progressively reduced for higher fluences and annealing temperatures as the size of the crystallites caused by irradiation and annealing increases. In addition, increased intermixing at the magnetic layer boundaries could alter the interface magnetostriction [62] (inversely proportional to the film thickness [63,64]), thus playing a role in the effective magnetostriction of the film.

Previous studies reported strong changes to the magnetoresistance after irradiation, in particular with heavy ions [32]. To validate the applicability of our irradiated permalloy layer for sensing applications, transport measurements are conducted. The AMR measurements are shown in Sec. S3 in Supplemental Material [36] for a full film as deposited and after irradiation with 5×10^{16} ions/cm^2. The electrical characterization confirms that the Ni-Fe-Cr(5 nm)/$Ni_{81}Fe_{19}$(30 nm)/Ta(4 nm) sample has sizable AMR, $\Delta R/R = 1.1(1)\%$. As the AMR does not change after irradiation with He^+ ions, the proposed material treatment is suitable for improving magnetic properties of magnetic material for magnetic sensing applications.

IV. CONCLUSIONS

In conclusion, we investigate the effects of He^+ irradiation and thermal annealing on the magnetic properties of Ni-Fe-Cr(5 nm)/$Ni_{81}Fe_{19}$(30 nm)/Ta(4 nm). Our XRD analysis suggests that both irradiation and annealing promote crystalline growth of the textured $Ni_{81}Fe_{19}$ alloy. While the irradiation treatment strongly reduces the hard-axis coercivity to 0.05 mT and the deposition-induced anisotropy by a factor of 10, the field-free annealing does not significantly improve the magnetic softness. We mainly attribute this to stress relaxation in the film after irradiation and to the different mechanism for atomic ordering, which is completely isotropic in the case of irradiation only. In addition, the effective magnetostriction of the film is reduced by a factor of 10 after irradiation and annealing as confirmed by anisotropy measurements in the presence of in-plane strain. Importantly, we show that the sizable magnetoresistance is preserved after the irradiation. As a result, postgrowth He^+ irradiation is an excellent tool to improve magnetic softness and minimize strain cross-sensitivity of permalloy. In contrast to thermal annealing, ion irradiation offers the advantage of performing a local material treatment [21,45,65] to adjust the anisotropy and write magnetic domain patterns directly into thin-film structured devices. As a consequence, we can locally tune the properties of a magnetic material to make it suitable, for instance, for high-sensitivity and low-hysteresis integrated AMR sensors that are insensitive to strain.

ACKNOWLEDGMENTS

This work has received funding from the European Union's Horizon 2020 research and innovation program under Marie Skłodowska-Curie Grant Agreement No. 860060 ["Magnetism and the Effect of Electric Field" (MagnEFi)], the Deutsche Forschungsgemeinschaft (DFG; TRR 173, 268565370, projects A01 and B02), the DFG-funded Collaborative Research Center 1261 (project A1), and the Austrian Research Promotion Agency (FFG). The authors acknowledge support by the chip production facilities of Sensitec GmbH (Mainz, Germany), where part of this work was performed, and the Max Planck Graduate Center with Johannes Gutenberg University Mainz.

[1] M. A. Khan, J. Sun, B. Li, A. Przybysz, and J. Kosel, Magnetic sensors-a review and recent technologies, Eng. Res. Express **3**, 022005 (2021).

[2] W. Kwiatkowski and S. Tumanski, The permalloy magnetoresistive sensors-properties and applications, J. Phys. E: Sci. Instrum. **19**, 502 (1986).

[3] J. Groenland, C. Eijkel, J. Fluitman, and R. de Ridder, Permalloy thin-film magnetic sensors, Sens. Actuators A: Phys. **30**, 89 (1992).

[4] J. Trützschler, K. Sentosun, M. Langer, I. Mönch, R. Mattheis, J. Fassbender, and J. McCord, Optimization of magneto-resistive response of ion-irradiated exchange biased films through zigzag arrangement of magnetization, J. Appl. Phys. **115**, 103901 (2014).

[5] L. Jogschies, D. Klaas, R. Kruppe, J. Rittinger, P. Taptimthong, A. Wienecke, L. Rissing, and M. C. Wurz, Recent developments of magnetoresistive sensors for industrial applications, Sensors **15**, 28665 (2015).

[6] K.-M. Lenssen, D. Adelerhof, H. Gassen, A. Kuiper, G. Somers, and J. Van Zon, Robust giant magnetoresistance sensors, Sens. Actuators A: Phys. **85**, 1 (2000).

[7] G. S. Cañón Bermúdez and D. Makarov, Magnetosensitive E-Skins for interactive devices, Adv. Funct. Mater. **31**, 2007788 (2021).

[8] E. S. Oliveros Mata, G. S. Cañón Bermúdez, M. Ha, T. Kosub, Y. Zabila, J. Fassbender, and D. Makarov, Printable anisotropic magnetoresistance sensors for highly compliant electronics, Appl. Phys. A **127**, 1 (2021).

[9] M. Melzer, D. Makarov, and O. Schmidt, A review on stretchable magnetic field sensorics, J. Phys. D: Appl. Phys. **53**, 083002 (2019).

[10] S. Amara, G. A. T. Sevilla, M. Hawsawi, Y. Mashraei, H. Mohammed, M. E. Cruz, Y. P. Ivanov, S. Jaiswal, G. Jakob, and M. Kläui, *et al.*, High-performance flexible magnetic tunnel junctions for smart miniaturized instruments, Adv. Eng. Mater. **20**, 1800471 (2018).

[11] G. Wang, C. Dong, W. Wang, Z. Wang, G. Chai, C. Jiang, and D. Xue, Observation of rotatable stripe domain in permalloy films with oblique sputtering, J. Appl. Phys. **112**, 093907 (2012).

[12] T. Iwata and F. Hagedorn, Annealing behavior of induced anisotropy and related magnetic properties in permalloy films, J. Appl. Phys. **40**, 2258 (1969).

[13] X. Jiang, X. Fan, J. Huang, C. Zhang, and D. Xue, Improving the quality of AMR of permalloy films by N^{2+} ion irradiation, Nucl. Instrum. Methods Phys, Res. Sect. B: Beam Interact. Mater. At. **430**, 54 (2018).

[14] M. Jaafar, R. Sanz, J. McCord, J. Jensen, R. Schäfer, M. Vázquez, and A. Asenjo, Pattern-induced magnetic anisotropy in FePt thin films by ion irradiation, Phys. Rev. B **83**, 094422 (2011).

[15] T. Devolder, I. Barisic, S. Eimer, K. Garcia, J.-P. Adam, B. Ockert, and D. Ravelosona, Irradiation-induced tailoring of the magnetism of CoFeB/MgO ultrathin films, J. Appl. Phys. **113**, 203912 (2013).

[16] D. Ravelosona, C. Chappert, V. Mathet, and H. Bernas, Chemical order induced by ion irradiation in FePt (001) films, Appl. Phys. Lett. **76**, 236 (2000).

[17] G. Masciocchi, J. W. van der Jagt, M.-A. Syskaki, A. Lamperti, N. Wolff, A. Lotnyk, J. Langer, L. Kienle, G. Jakob, B. Borie, A. Kehlberger, D. Ravelosona, and M. Kläui, Control of magnetoelastic coupling in Ni/Fe multilayers using He^+ ion irradiation, Appl. Phys. Lett. **121**, 182401 (2022).

[18] M. C. H. de Jong, M. J. Meijer, J. Lucassen, J. van Liempt, H. J. M. Swagten, B. Koopmans, and R. Lavrijsen, Local control of magnetic interface effects in chiral Ir— Co— Pt multilayers using Ga^+ ion irradiation, Phys. Rev. B **105**, 064429 (2022).

[19] X. Zhao, B. Zhang, N. Vernier, X. Zhang, M. Sall, T. Xing, L. H. Diez, C. Hepburn, L. Wang, and G. Durin, *et al.*, Enhancing domain wall velocity through interface intermixing in W-CoFeB-MgO films with perpendicular anisotropy, Appl. Phys. Lett. **115**, 122404 (2019).

[20] L. H. Diez, M. Voto, A. Casiraghi, M. Belmeguenai, Y. Roussigné, G. Durin, A. Lamperti, R. Mantovan, V. Sluka, and V. Jeudy, *et al.*, Enhancement of the Dzyaloshinskii-Moriya interaction and domain wall velocity through interface intermixing in Ta/CoFeB/MgO, Phys. Rev. B **99**, 054431 (2019).

[21] S. Woods, S. Ingvarsson, J. Kirtley, H. Hamann, and R. Koch, Local magnetic anisotropy control in NiFe thin films via ion irradiation, Appl. Phys. Lett. **81**, 1267 (2002).

[22] A. Schindler, R. Kernohan, and J. Weertman, Effect of irradiation on magnetic properties of Fe-Ni alloys, J. Appl. Phys. **35**, 2640 (1964).

[23] A. Mougin, T. Mewes, M. Jung, D. Engel, A. Ehresmann, H. Schmoranzer, J. Fassbender, and B. Hillebrands, Local manipulation and reversal of the exchange bias field by ion irradiation in FeNi/FeMn double layers, Phys. Rev. B **63**, 060409(R) (2001).

[24] J. Trützschler, K. Sentosun, B. Mozooni, R. Mattheis, and J. McCord, Magnetic domain wall gratings for magnetization reversal tuning and confined dynamic mode localization, Sci. Rep. **6**, 30761 (2016).

[25] J. Fassbender, J. von Borany, A. Mücklich, K. Potzger, W. Möller, J. McCord, L. Schultz, and R. Mattheis, Structural and magnetic modifications of Cr-implanted permalloy, Phys. Rev. B **73**, 184410 (2006).

[26] J. Fassbender and J. McCord, Control of saturation magnetization, anisotropy, and damping due to Ni implantation in thin NiFe layers, Appl. Phys. Lett. **88**, 252501 (2006).

[27] J. Fassbender, A. Mücklich, K. Potzger, and W. Möller, Mixing and subsequent amorphization of ultrathin NiFe/Ta bilayers by 30 keV Ni implantation, Nucl. Instrum. Methods Phys. Res. Sect. B: Beam Interact. Mater. At. **248**, 343 (2006).

[28] G. C. Bailey, A. I. Schindler, and P. H. Meijer, Ferromagnetic resonance of ^{3}He-irradiated thin metal films, J. Appl. Phys. **38**, 4004 (1967).

[29] G. Bailey, Dependence of spin-wave resonance in thin films on irradiation, Phys. Lett. A **30**, 58 (1969).

[30] R. Gupta, K. Lieb, Y. Luo, G. Müller, P. Schaaf, and K. Zhang, Argon and krypton ion-induced changes in permalloy thin films, Eur. Phys. J. B **63**, 501 (2008).

[31] J. Fassbender, D. Ravelosona, and Y. Samson, Tailoring magnetism by light-ion irradiation, J. Phys. D: Appl. Phys. **37**, R179 (2004).

[32] J. Baglin, M. Tabacniks, R. Fontana, A. Kellock, and T. Bardin, in *Materials Science Forum*, Vol. 248 (Trans Tech Publ, 1997), p. 87.

[33] W. Lee, M. Toney, and D. Mauri, High magnetoresistance in sputtered Permalloy thin films through growth on seed layers of $(Ni_{0.81}Fe_{0.19})_{1-x}/Cr_x$, IEEE Trans. Magn. **36**, 381 (2000).

[34] J. F. Ziegler, M. D. Ziegler, and J. P. Biersack, SRIM – the stopping and range of ions in matter (2010), Nucl. Instrum. Methods Phys. Res. Sect. B: Beam Interact. Mater. At. **268**, 1818 (2010).

[35] J. Vukanić and P. Sigmund, Total backscattering of keV light ions from solid targets in single-collision approximation, Appl. Phys. **11**, 265 (1976).

[36] See Supplemental Material at http://link.aps.org/supplemental/10.1103/PhysRevApplied.20.014001 for the X-ray-diffraction rocking-curve measurements, the TRIM simulations, AMR measurements, and magnetic hysteresis loops after annealing at different temperatures.

[37] C. Okay, P. Aksu, C. Deger, and F. Yildiz, Tailoring the magnetic anisotropy of cobalt-gold thin films, Turk. J. Phys. **42**, 335 (2018).

[38] E. Klokholm and J. Aboaf, The saturation magnetostriction of permalloy films, J. Appl. Phys. **52**, 2474 (1981).

[39] G. Masciocchi, M. Fattouhi, A. Kehlberger, L. Lopez-Diaz, M.-A. Syskaki, and M. Kläui, Strain-controlled domain wall injection into nanowires for sensor applications, J. Appl. Phys. **130**, 183903 (2021).

[40] A. Raghunathan, J. E. Snyder, and D. Jiles, Comparison of alternative techniques for characterizing magnetostriction and inverse magnetostriction in magnetic thin films, IEEE Trans. Magn. **45**, 3269 (2009).

[41] M. Ahmadipour, M. J. Abu, M. F. Ab Rahman, M. F. Ain, and Z. A. Ahmad, Assessment of crystallite size and strain of $CaCu_3Ti_4O_{12}$ prepared via conventional solid-state reaction, Micro Nano Lett. **11**, 147 (2016).

[42] A. K. Zak, W. A. Majid, M. E. Abrishami, and R. Yousefi, X-ray analysis of ZnO nanoparticles by Williamson-Hall and size-strain plot methods, Solid State Sci. **13**, 251 (2011).

[43] V. Speriosu and T. Vreeland Jr, X-ray rocking curve analysis of superlattices, J. Appl. Phys. **56**, 1591 (1984).

[44] S. Park, D. Norton, and V. Selvamanickam, Ion-beam texturing of uniaxially textured Ni films, Appl. Phys. Lett. **87**, 031907 (2005).

[45] J. McCord, T. Gemming, L. Schultz, J. Fassbender, M. O. Liedke, M. Frommberger, and E. Quandt, Magnetic anisotropy and domain patterning of amorphous films by He-ion irradiation, Appl. Phys. Lett. **86**, 162502 (2005).

[46] J. W. van der Jagt, V. Jeudy, A. Thiaville, M. Sall, N. Vernier, L. Herrera Diez, M. Belmeguenai, Y. Roussigné, S. M. Chérif, and M. Fattouhi, *et al.*, Revealing nanoscale disorder in W/Co-Fe-B/MgO ultrathin films using domain-wall motion, Phys. Rev. Appl. **18**, 054072 (2022).

[47] W. Wang, J. Jordan-Sweet, G. Miao, C. Ni, A. Rumaiz, L. Shah, X. Fan, P. Parsons, R. Stearrett, and E. Nowak, *et al.*, In-situ characterization of rapid crystallization of amorphous CoFeB electrodes in CoFeB/MgO/CoFeB junctions during thermal annealing, Appl. Phys. Lett. **95**, 242501 (2009).

[48] F. Schulz, R. Lawitzki, H. Głowiński, F. Lisiecki, N. Träger, P. Kuświk, E. Goering, G. Schütz, and J. Gräfe, Increase of Gilbert damping in permalloy thin films due to heat-induced structural changes, J. Appl. Phys. **129**, 153903 (2021).

[49] P. Zou, W. Yu, and J. A. Bain, Influence of stress and texture on soft magnetic properties of thin films, IEEE Trans. Magn. **38**, 3501 (2002).

[50] K. Y. Guslienko, V. Novosad, Y. Otani, H. Shima, and K. Fukamichi, Field evolution of magnetic vortex state in ferromagnetic disks, Appl. Phys. Lett. **78**, 3848 (2001).
[51] T. Wurft, W. Raberg, K. Prügl, A. Satz, G. Reiss, and H. Brückl, Evolution of magnetic vortex formation in micron-sized disks, Appl. Phys. Lett. **115**, 132407 (2019).
[52] R. Gupta, K.-H. Han, K. Lieb, G. Müller, P. Schaaf, and K. Zhang, Influence of ion implantation on the magnetic properties of thin FeCo films, J. Appl. Phys. **97**, 073911 (2005).
[53] L. Jian, J. Liu, and J. Mayer, Ar^{+} ion irradiation induced grain growth in Au and Pt thin films, Nucl. Instrum. Methods Phys. Res. Sect. B: Beam Interact. Mater. At. **36**, 306 (1989).
[54] J. C. Liu, M. Nastasi, and J. Mayer, Ion irradiation induced grain growth in Pd polycrystalline thin films, J. Appl. Phys. **62**, 423 (1987).
[55] J. C. Liu and J. Mayer, Ion irradiation induced grain growth in Ni polycrystalline thin films, Nucl. Instrum. Methods Phys. Res. Sect. B: Beam Interact. Mater. At. **19**, 538 (1987).
[56] T. Devolder, Light ion irradiation of Co/Pt systems: Structural origin of the decrease in magnetic anisotropy, Phys. Rev. B **62**, 5794 (2000).
[57] A. Maziewski, P. Mazalski, Z. Kurant, M. O. Liedke, J. McCord, J. Fassbender, J. Ferré, A. Mougin, A. Wawro, L. T. Baczewski, A. Rogalev, F. Wilhelm, and T. Gemming, Tailoring of magnetism in Pt/Co/Pt ultrathin films by ion irradiation, Phys. Rev. B **85**, 054427 (2012).
[58] S. Finizio, M. Foerster, M. Buzzi, B. Krüger, M. Jourdan, C. A. F. Vaz, J. Hockel, T. Miyawaki, A. Tkach, S. Valencia, F. Kronast, G. P. Carman, F. Nolting, and M. Kläui, Magnetic Anisotropy Engineering in Thin Film Ni Nanostructures by Magnetoelastic Coupling, Phys. Rev. Appl. **1**, 021001(R) (2014).
[59] I. Gilbert, A. C. Chavez, D. T. Pierce, J. Unguris, W.-Y. Sun, C.-Y. Liang, and G. P. Carman, Magnetic microscopy and simulation of strain-mediated control of magnetization in PMN-PT/Ni nanostructures, Appl. Phys. Lett. **109**, 162404 (2016).
[60] R. M. Bozorth, *Ferromagnetism, p. 263* (1993).
[61] J. W. Judy, Magnetic microactuators with polysilicon flexures, Masters Report (1994).
[62] E. Singleton and K. Duxstad, Interfacial contributions to magnetostriction of ferromagnetic layers for magnetoresistive sensors, MRS Online Proc. Library **721**, 1 (2002).
[63] G. Choe, Giant interface magnetostriction and temperature dependence in NiFe films encapsulated with Ta and AlOx layers, IEEE Trans. Magn. **35**, 3838 (1999).
[64] O. Song, C. Ballentine, and R. O'Handley, Giant surface magnetostriction in polycrystalline Ni and NiFe films, Appl. Phys. Lett. **64**, 2593 (1994).
[65] J. Fassbender and J. McCord, Magnetic patterning by means of ion irradiation and implantation, J. Magn. Magn. Mater. **320**, 579 (2008).